JOURNAL OF GEOPHYSICAL RESEARCH, VOL. 88, NO. C7, PAGES 4393–4406, MAY 20, 1983

# SEASAT Synthetic Aperture Radar Observations of Wave-Current and Wave-Topographic Interactions

G. A. MEADOWS,[1] R. A. SHUCHMAN, Y. C. TSENG,[2] AND E. S. KASISCHKE

*Environmental Research Institute of Michigan, Ann Arbor, Michigan 48107*

This study investigated the capability of a spaceborne, imaging radar system to detect subtle changes in the propagation characteristics of ocean wave systems. Specifically, an evolving surface gravity wave system emanating from Hurricane Ella and propagating toward Cape Hatteras, North Carolina, formed the basis of this investigation. This wave system was successfully imaged by the SEASAT synthetic aperture radar (SAR) during revolution 974 on September 3, 1978. Estimates of the dominant wavelength and direction of the ocean waves were derived from the SAR data by using optical Fourier transforms. Environmental data of the test area, which included the surface velocity vector within the Gulf Stream, the location of Hurricane Ella, and local bathymetric information, were used in conjunction with the SAR data to form the basis of this comparative study. Favorable agreement was found between wave rays calculated by utilizing theoretical wave-current and wave-topographic interactions and SAR observed dominant wavelength and direction changes across the Gulf Stream and continental shelf.

## INTRODUCTION

Investigation of the backscatter of microwave energy from the sea surface provides a unique way to view large spatial regions of the ocean nearly simultaneously. Synoptic views of open-ocean wave characteristics as provided from the SEASAT synthetic aperture radar (SAR) allow study of the generation, propagation, and physical characteristics of an evolving wave train across the sea surface. Since the intensity of radar backscatter can be related to the characteristics of ocean wave propagation [*Gonzalez et al.*, 1979; *Shuchman and Meadows*, 1980; *Schwab et al.*, 1981; *Meadows et al.*, 1982], definitive information is now available concerning the generation, propagation, and dynamic interaction of these surface wave motions with the upper regions of the ocean.

In an effort to quantify the dynamic interaction of hurricane-generated, surface gravity waves with a major ocean current system, and eventually with the rising ocean bottom in the coastal region, SEASAT SAR data from revolution 974 were analyzed. Data collected from the western North Atlantic off Cape Hatteras, N.C., were utilized to investigate the interaction of the Gulf Stream with an ocean surface gravity wave field.

The overall objective of this study was to utilize the wave information obtainable from SEASAT SAR imagery to document the complex oceanographic conditions responsible for wave transformations observed on SAR imagery collected during revolution 974. The source of the waves, Hurricane Ella, was identified both from meteorological records as well as by wave hindcast projections. Wave rays from this source were then constructed. Using the kinematic wave/current interaction theory of *Phillips* [1981], these projected wave rays were refracted through the Gulf Stream and were statistically compared to the observed set of wave rays constructed from SAR-observed wave directions. Finally, using inputs from the deepwater analysis, several shallow water wave refraction models were run, and the results from these models were compared to SAR observed data.

## DATA DESCRIPTION AND ANALYSIS METHODS

The data utilized in this investigation were collected by the SEASAT satellite. Among the instrumentation carried by SEASAT, which was launched during June 1978, was a synthetic aperture radar (SAR). This satellite collected over 500 passes of SAR data before suffering a catastrophic power loss in October 1978. The SAR onboard SEASAT was an *L* band (23.5-cm wavelength) radar [see *Jordan*, 1980, or *Beal et al.*, 1981]. It collected 25 × 25 m resolution imagery and viewed a ground swath width of 100 km and a length of up to 4000 km; it viewed the surface of the earth with an average incident angle of 20°.

Synthetic aperture radar is a coherent radar that uses the motion of a moderately broad physical antenna beam to synthesize a very narrow beam, thus providing fine azimuthal (along-track) resolution [*Brown and Porcello*, 1969; *Harger*, 1970]. Fine range (cross-track) resolution is achieved by transmitting either very short pulses or longer coded pulses that are compressed by matched-filtering techniques into equivalent short pulses. Usually, the coded pulse is a waveform linearly modulated in frequency.

Analysis of the SEASAT SAR ocean wave data set collected during revolution 924 included the documentation and evaluation of four phenomena associated with the ocean surface gravity wave system as it propagated toward Cape Hatteras. The analysis included: (1) location of the generation region of these wave trains by hindcast projections; (2) evaluation of the limits of detectability of the SEASAT SAR to sense subtle changes of ocean surface wave propagation direction and wave number for a spatially evolving gravity wave system; (3) measurement of the effect of a major ocean current system (the Gulf Stream) on the propagation characteristics of these surface waves; and (4) evaluation of the potential of SEASAT SAR to accurately map the magnitude and direction of major ocean current systems from the observed wave/current interaction.

The successful completion of these four tasks can be largely attributed to the recent development of two, ocean remote sensing tools. These are an analytical wave/current interaction model, initially developed by *Phillips* [1981], and refinement of two-dimensional, optical Fourier transform (OFT) techniques applied to ocean wave remote sensing [*Shuchman et al.*, 1979].

[1]Department of Atmospheric and Oceanic Science, University of Michigan, Ann Arbor, MI 48109.
[2]Department of Atmospheric and Oceanic Science, University of Michigan Ann Arbor, MI 48109.

Copyright 1983 by the American Geophysical Union.

Paper number 2C1908.
0148-0227/83/002C-1908$05.00

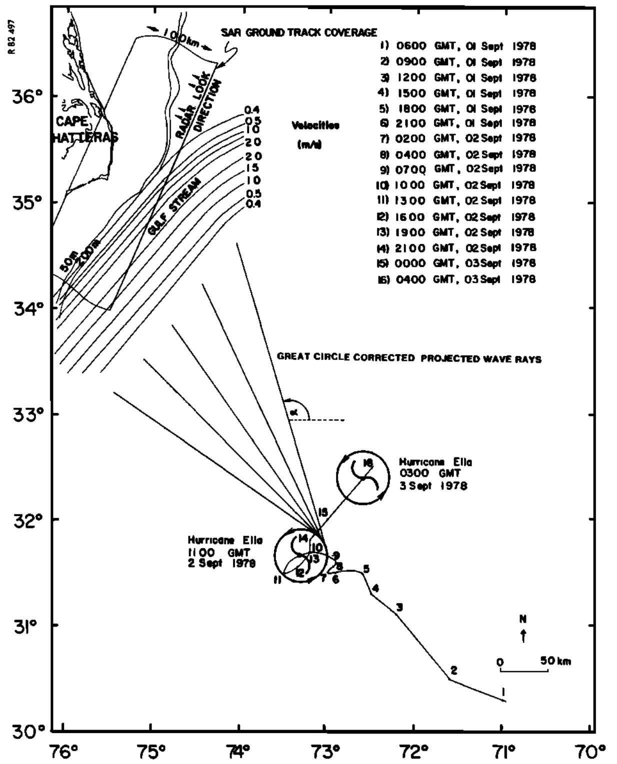


Fig. 1. Ground swath coverage of the SEASAT SAR, the location of the Gulf Stream off Cape Hatteras, North Carolina, and the storm track and location of Hurricane Ella at the time of satellite overpass.

These techniques have been utilized to investigate the spatial evolution of surface gravity wave propagation.

Figure 1 outlines the test site and shows the ground swath coverage of the SEASAT SAR, the location of the Gulf Stream, and the location of Hurricane Ella. Note that the hurricane was moving in a northeasterly direction, and it is this storm center that generated the waves that propagated toward Cape Hatteras. The characteristics of this wave field as it was altered by the Gulf Stream and the local bottom topography were studied in detail with the use of optical Fourier transform analysis techniques.

A set of 116 optical Fourier transforms were generated from the SEASAT SAR data in order to investigate the observed changes in surface gravity wave propagation characteristics in deepwater regions off Cape Hatteras. The areas transformed were from the first 50 km of the swath from revolution 974; their locations are summarized in Figure 2. The positions are separated 12.5 km in the azimuth direction and 10 km in the range direction. The circular aperture utilized to generate the OFTs had an equivalent ground size of 44 km$^2$, or covered approximately 40 cycles of wave data.

Previous investigations [*Shuchman et al.*, 1981; *Vesecky and Stewart*, 1982; *Gonzalez et al.*, 1979] have successfully demonstrated that optical Fourier transform techniques can be applied to SEASAT SAR data to extract reliable estimates of dominant wavelength and propagation direction of an imaged gravity wavefield. This demonstration was realized by comparing the OFT estimates with coincident in situ wave measurements. The present analysis utilized OFT techniques on optically processed SEASAT data to estimate only the dominant wavelength and direction of propagation. No attempt was made to use the entire gravity wave spectral estimate provided by the OFT, nor do the authors presume that the OFTs can be readily interpreted to provide power spectral density information of the ocean surface. Digitally processed SEASAT data and the use of fast Fourier transform (FFT) spectral analysis techniques may yield even better comparisons between the SAR-derived spectral estimates and oceanographic theory.

From the optical Fourier transforms, estimates of dominant wavelength and direction were obtained by conventional means [*Shuchman et al.*, 1979]. Dominant wavelength and direction were not detectable on all the OFTs; estimates of dominant wavelength were obtained from 99 positions and wave directions from 101 positions.

Bathymetric data utilized in this investigation were obtained from two primary sources. The first source was U.S. coastal hydrographic data obtained from the National Oceanic and Atmospheric Administration's (NOAA) National Geophysical and Solar-Terrestrial Data Center in Boulder, Colorado. These data were digitized from National Ocean Survey (NOS) Smooth Sheets dating from 1930 to 1973. The other source was NOAA and Defense Mapping Agency (DMA) navigational charts.

The position as well as the velocity of the Gulf Stream is temporally varying. Historical observations of Gulf Stream meander, reported by *Fuglister and Worthington* [1951], indicate the Gulf Stream shifts its position in an easterly or westerly direction at a rate of approximately 20 km/d. Early estimates of the Gulf Stream surface velocity range from values of 1–1.2 m/s by the dynamic computation method [*Iselin*, 1936] to values of 2–2.5 m/s by Loran system and bathythermography [*Iselin and Fuglister*, 1948]. Other investigators [*Worthington*, 1954; *Von Arx*, 1962] also found that the maximum surface speed is around 2 m/s. The speed decreases gradually across the Gulf Stream toward both boundaries from a maximum near the center. In general the rate of decrease is slower in the outer (eastern) side than in the inner (western) side of the stream. The United States Coast Guard Oceanographic Unit publishes weekly sea current charts for specific areas, which include the Gulf Stream region. These charts are produced by a subjective analysis of all available data, which include bathythermographs (BT), airborne radiation thermometry (ART), satellite slope files, shelf files, and other miscellaneous sources, such as weather charts and current charts produced by other agencies.

To investigate wave/current interactions across the Gulf Stream, this study utilized available sea truth, consisting of the weekly sea current chart prepared by the U.S. Coast Guard on August 30, 1978 [*U.S. Coast Guard*, 1978]. The Gulf Stream position and profile presented in Figure 1 was reproduced from the southwestern part of this chart. The maximum current speed of 2 m/s is located in the center portion of the stream and decreases gradually toward either side. It also shows that the cross-stream spatial gradient in current speed is lower toward the outer boundary than toward the inner boundary.

The surface gravity wave fields studied in this investigation were generated by Hurricane Ella. Based upon a detailed, surface meteorological analysis, it was determined that Hurricane Ella was situated southeast of the Gulf Stream at about latitude 32°30'N and longitude 72°30'W, moving toward the northeast when the SEASAT SAR imaged the Cape Hatteras region on September 3, 1978 (see Figure 1). However, since the hurricane-generated waves require time to propagate to the Gulf Stream, the hurricane position, from which these waves were generated, would have been southwest of the above-mentioned position. These waves were found to be generated at a hurricane radius of 30 km (a little less than 1.5 times the radius of maximum wind velocity [*Ross*, 1981]) and propagating with a calculated

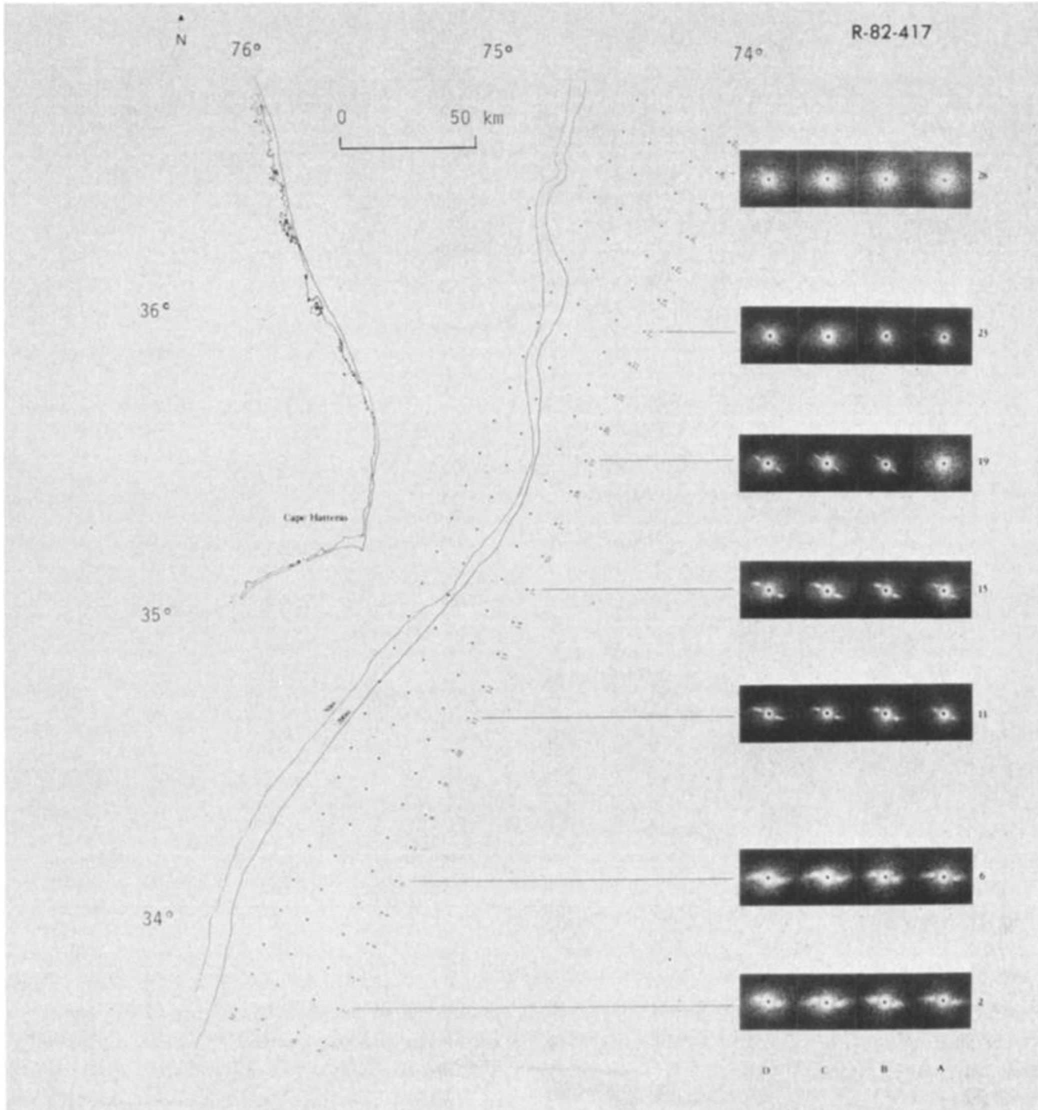


Fig. 2. The positions of the 116 optical Fourier transforms from the deepwater regions off Cape Hatteras obtained from SEASAT revolution 974, plus several examples of OFT's.

average group velocity of 30 km/h in a tangential direction to the hurricane radius. This group velocity was calculated from the wave number of peak energy measured by the SEASAT SAR near the outer boundary of the Gulf Stream. The required travel time from the above-mentioned hurricane center to the outer boundary of the Gulf Stream, in the southern portion of the study area, is approximately 10 hours. This time period allows us to locate, from the trace of the hurricane center, the actual area responsible for wave generation. This actual center is located at latitude 31°30′N and longitude 73°14′W. The input sea conditions (wave rays) were obtained from the extension of the tangential lines from a circle of radius 30 km from this hurricane center. The position of Hurricane Ella at the estimated time of wave propagation into the northern sector of Cape Hatteras, along with the projected wave rays, is also presented in Figure 1. Note that these projected wave rays do not include the effect of wave/current interaction after entering the Gulf Stream but do include effects of earth curvature on their propagation paths.

A shallow water (< 200-m depth), bathymetrically controlled refraction analysis was also performed on the wave field from Hurricane Ella that had been refracted by the Gulf Stream and had emerged from the western edge of the Stream. Using dominant wavelengths and directions determined by the deepwater analysis as inputs, two shallow water wave refraction models were run. The shallow water wavelengths and directions obtained from these models were statistically compared to SAR-derived shallow water estimates.

The position of the 116 optical Fourier transforms from the deepwater regions off Cape Hatteras, obtained from SEASAT revolution 974, plus several examples of OFT's obtained from the SAR data, are presented in Figure 2. From Figure 2 it can be observed that in the southern portion of the pass (rows 1–11) the direction of the waves is nearly perpendicular to the SAR flight direction, whereas in the northern portion (rows 19–29) the waves are traveling 30°–45° off perpendicular. A representative summary of the position, the OFT-estimated dominant wavelength and direction, and the water depth at each point is presented in Table 1. (For a complete presentation of the OFT analysis, see *Kasischke et al.* [1981].)

From Table 1 it is clear that there are significant changes occurring in the deepwater dominant wavelength and direction at the time SEASAT made its overflight. Two factors were considered as the source of this variation: (1) a wave/current

TABLE 1. Summary of Representative SAR-Derived Dominant Wavelength and Direction of Deepwater Areas Found on Revolution 974

| Position | Latitude | Longitude | Water Depth, m | Wavelength, m | Wave Direction, °T |
|---|---|---|---|---|---|
| 2A | 34°43′ | 75°39′ | >1000 | 176.2 | 306.0 |
| 2B | 34°44′ | 75°41′ | >1000 | 180.8 | 310.5 |
| 2C | 34°47′ | 75°50′ | >1000 | 176.2 | 306.0 |
| 2D | 34°49′ | 75°56′ | >1000 | 180.8 | 305.5 |
| 6A | 35°08′ | 75°25′ | >1000 | 180.8 | 305.0 |
| 6B | 35°09′ | 75°34′ | >1000 | 190.8 | 307.0 |
| 6C | 35°12′ | 75°39′ | >1000 | 176.2 | 305.5 |
| 6D | 35°14′ | 75°46′ | >1000 | 180.0 | 305.0 |
| 11A | 34°39′ | 75°07′ | >1000 | 202.1 | 317.5 |
| 11B | 34°41′ | 75°13′ | >1000 | 190.8 | 318.0 |
| 11C | 34°44′ | 75°22′ | >1000 | 196.3 | 317.5 |
| 11D | 34°48′ | 75°28′ | >1000 | 196.3 | 315.5 |
| 15A | 35°05′ | 74°53′ | >1000 | 196.3 | 326.0 |
| 15B | 35°07′ | 74°59′ | >1000 | 196.3 | 321.5 |
| 15C | 35°10′ | 75°08′ | 75.0 | 190.8 | 322.0 |
| 15D | 35°13′ | 75°14′ | 18.3 | 159.8 | 319.5 |
| 19A | 35°31′ | 74°39′ | >1000 | 208.2 | 334.0 |
| 19B | 35°33′ | 74°45′ | >1000 | 190.8 | 331.0 |
| 19C | 35°36′ | 74°54′ | 58.6 | 167.6 | 325.5 |
| 19D | 35°39′ | 75°00′ | 51.2 | 171.8 | 321.5 |
| 23A | 35°57′ | 74°25′ | >1000 | — | — |
| 23B | 35°58′ | 74°31′ | >1000 | 190.8 | 350.0 |
| 23C | 36°02′ | 74°40′ | >1000 | 180.8 | 345.5 |
| 23D | 36°04′ | 74°47′ | 119.0 | 190.8 | 352.0 |
| 28A | 36°28′ | 74°07′ | >1000 | — | — |
| 28B | 36°30′ | 74°13′ | >1000 | — | — |
| 28C | 36°33′ | 74°23′ | >1000 | 221.7 | 353.0 |
| 28D | 36°35′ | 74°29′ | >1000 | 214.8 | 352.5 |

*Dash indicates no data extractable from OFT.

interaction between the Gulf Stream and the incident gravity wave field and (2) spatial variations in the evolving gravity wave field from its hurricane source.

## THEORY OF WAVE/CURRENT INTERACTION

Gravity waves propagating across the ocean surface generally experience a variety of weak and strong interactions [*Phillips*, 1981]. These interactions may occur between other surface waves of the same wave train [*Lake and Yuen*, 1978; *Yuen and Lake*, 1980], with waves from different generating regions [*Longuet-Higgins and Stewart*, 1960; *Longuet-Higgins*, 1978; *Phillips*, 1981], or with other dynamic conditions of the upper ocean, such as major current systems [*Kenyon*, 1971; *Peregrine*, 1976; *Hayes*, 1981], large-scale eddies, or bottom topographic features [*Shuchman*, 1982]. As a result of these interactions the propagation characteristics of the incident surface gravity wave field will be altered. Refraction as well as reflection of wave components may occur as a result of strong interactions between an incident ocean surface gravity wave field and a major ocean current system such as the Gulf Stream.

Consider a surface gravity wave field propagating across the Gulf Stream in deep water of uniform depth. The Gulf Stream is assumed to be in steady state (compared to the travel time of a wave group across the stream) with slightly varying velocities across it. The minimum velocity occurs at both boundaries of the stream, while the maximum velocity is in the center portion. For the purposes of this investigation the Gulf Stream velocity profile was assumed uniform with depth. Review of current profiles with depth through the Gulf Stream in the region of Cape Hatteras, provided by *Fuglister* [1963] and by *Richardson and Knauss* [1971], indicate a maximum vertical shear of $2.75 \times 10^{-3}$ s$^{-1}$. This maximum value of vertical shear for the upper region of the Gulf Stream is approximately 8 times smaller than that experienced by the vertical decay of the wave-induced motions within the same region. Hence, the kinematic effect of vertical variations in the Gulf Stream flow profile was neglected in this analysis. These assumptions are generally justified by the Gulf Stream flow field in the region near Cape Hatteras. The methodology utilized in this investigation parallels the wave/current interaction theory presented by *Phillips* [1981]; thus only a brief summary of this development will be presented.

To first order, the propagation of surface waves in water of uniform depth $d$ and with constant atmospheric pressure is given by the following dispersion relation:

$$\sigma^2(k) = k(g + \gamma k^2) \tanh kd \tag{1}$$

where $k = |\mathbf{k}|$, $\mathbf{k}$ is the vector wave number $(k_1, k_2)$, $g$ is the gravitational acceleration, $\gamma$ is the ratio of surface tension to water density, and $\sigma$ is the intrinsic frequency. In deep water the water depth is much larger than the wavelength, and $kd$ is much larger than unity. Gravity waves are those whose restoring force is mainly due to gravity and which have wavelengths greater than $2\pi(\gamma/g)^{1/2}$. For deepwater gravity waves the dispersion relation (1), neglecting surface tension and invoking the deepwater assumption, reduces to

$$\sigma^2 = gk \tag{2}$$

For surface gravity waves moving in a medium with a velocity $u$ relative to an observation point, the observed or apparent frequency of waves $n$ measured at a fixed point should include a Doppler shift to the intrinsic frequency:

$$n = \sigma(\mathbf{k}) + \mathbf{k} \cdot \mathbf{u} \tag{3}$$

where $\mathbf{u}$ is the velocity vector of the current (assumed constant with depth).

For waves riding on or across a current with slowly changing velocities $u(y)$, as shown in Figure 3, the angles $\alpha_i$ are the incident angles or refraction angles. When the waves are incident upon the current from a region with average velocity $u_0$ to a region with average velocity $u_1$, the shear per unit distance is $u_1 - u_0$, and the conservation of wave frequency becomes

$$\sigma_0 = \sigma_1 + k_1(u_1 - u_0) \cos \alpha_1 \tag{4}$$

and the conservation of wave numbers is given by *Phillips* [1981] as

$$k_0 \cos \alpha_0 = k_1 \cos \alpha_1 = \text{constant} \tag{5}$$

Expressing (4) in terms of $\alpha_1$ gives

$$\cos \alpha_1 = \frac{\sigma_0 - \sigma_1}{k_1(u_1 - u_0)} = K_1/k_1 \tag{6}$$

and substituting $k_1$ from (5) into (6) gives

$$\cos \alpha_0 = \frac{\sigma_0 - \sigma_1}{k_0(u_1 - u_0)} = K_1/k_0 \tag{7}$$

where $K_1 = (\sigma_0 - \sigma_1)/(u_1 - u_0)$, and for deepwater gravity waves the dispersion relation is $\sigma = gk$. Theoretically, the incident and refraction angles can be calculated from (6) and (7) when both the shear of the current and the wave numbers in two adjacent regions of the current are known.

Equations (4) and (5) have been reduced to another useful presentation [*Phillips*, 1981]:

$$\cos \alpha_1 = \frac{gk_0 \cos \alpha_0}{[\sigma_0 - k_0(u_1 - u_0) \cos \alpha_0]^2} \tag{8}$$

or

$$\cos \alpha_1 = \frac{\cos \alpha_0}{\left(1 - \dfrac{u_1 - u_0}{c_0} \cos \alpha_0\right)^2} \tag{9}$$

where $c_0 = (g/k_0)^{1/2}$ is the initial phase velocity of the wave train, and the term $(u_1 - u_0)/c_0 \cos \alpha_0$ is usually much less than unity. This term can be positive or negative, depending on the signs of $(u_1 - u_0)$ and $\cos \alpha_0$. If the incident angle $\alpha_0$ is less than 90°, the wave ray will turn away from its normal when it is traveling across a slowly increasing current; otherwise, if the wave is traveling across a slowly decreasing current, the wave ray will shift toward its normal. Similarly, if $\alpha_0$ is greater than 90°, the wave ray will turn toward or away from its normal, depending on an increasing or a decreasing current, respectively. For a particular critical incident angle, when the refraction angle becomes zero, the wave no longer penetrates further into the current but is reflected by the current. The condition of total reflection of the wave ray is obtained by setting $\alpha_1 = 0$ in (9) or $(u_1 - u_0)/c_0 = [1 - (\cos^{1/2} \alpha_0)]/\cos \alpha_0$. For small incident angles, even a small shear will result in reflection.

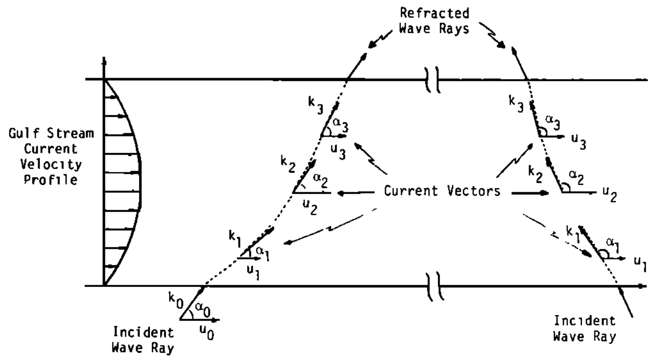


Fig. 3. Schematic representation of wave/current interaction and coordinate system utilized.

## COMPARISON OF SAR-DERIVED DOMINANT WAVELENGTH AND DIRECTION TO OCEANOGRAPHIC THEORY

The previous theoretical development of deepwater, kinematic wave/current interaction was applied to the SEASAT SAR-observed changes in deepwater gravity wave propagation in the region of the Gulf Stream. Figure 4 depicts the direction of travel of the dominant gravity wave components resolved by the OFT analysis of the SAR signal output imagery. Well-resolved, two-dimensional estimates of wave characteristics were obtained at these 101 positions (well-defined wave characteristics were not resolved on 15 of the OFT's). Average wave rays across the SAR swath were obtained by spatial averaging of wave direction obtained from adjacent OFT's.

This SEASAT SAR-observed wave ray plot over the spatial domain of the satellite overpass was utilized for three comparative analyses. First, the wave rays determined from the OFT analysis were hindcast to locate the wave generation region of Hurricane Ella. Second, they were compared to the projected wave rays from Hurricane Ella without consideration of the Gulf Stream. Finally, the SAR-observed wave rays were compared to wave rays constructed by using *Phillips'* [1981] wave/current model. In all cases, corrections for earth curvature were included in the calculations.

Figure 5 shows the result of the wave ray hindcast projections to locate the wave generation region of Hurricane Ella. These wave rays fall into two general groupings of approximately 50 × 50 km dimensions. The southernmost group (A) was derived from waves incident in the northern region of Cape Hatteras. The northern group of hindcast rays (B) originated from the southernmost OFT's. It is interesting to note that the spatial separation of these two groupings corresponds to the required wave group travel time (approximately 30.2 km/h) from the hurricane position to the OFT-sensed positions at the time of satellite overpass. These projections agree well with the hurricane positions reported for the day in question by the National Weather Service.

Utilizing the reported storm track of Hurricane Ella and the radius of maximum wave generation as the source of the gravity wave field (D. B. Ross, personal communication, 1981), great circle wave rays were constructed from the wave-generation region to the Cape Hatteras coast. These constructed wave rays, which did not include any surface current effects, were compared to the SAR-derived wave rays. These comparisons were poor and, hence, necessitated the inclusion of Gulf Stream wave/current interaction effects into the analysis.

As deepwater gravity waves propagate from the relatively undisturbed ocean and enter the Gulf Stream, their direction of

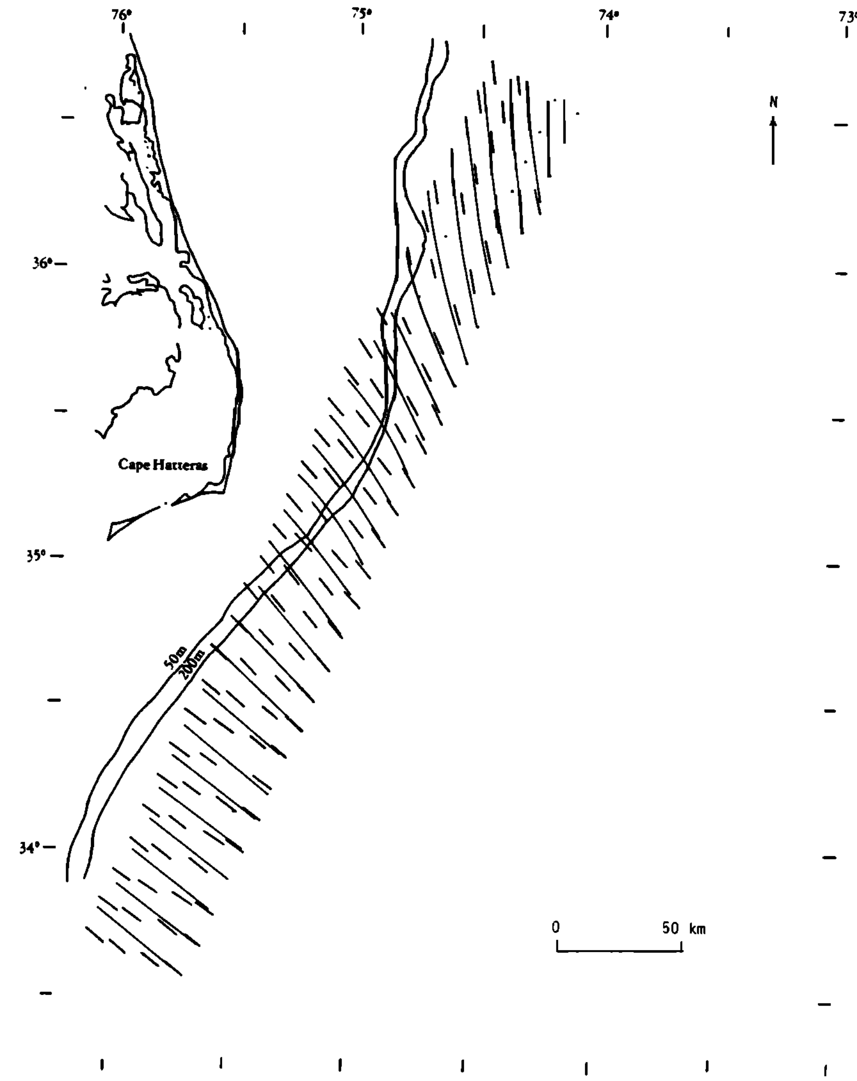


Fig. 4. Direction of dominant gravity wave components as derived from the SEASAT SAR and their corresponding spatially averaged wave rays.

propagation and wavelength will change. The refraction angle and resultant direction will depend mainly on the current shear, the wave number, and incident angle of the wave rays.

By identifying Hurricane Ella as the source of the gravity wave field present in the deepwater regions east of Cape Hatteras, and by simultaneously tracking these waves over a large distance (on the order of 500 km), we have successfully identified the major source of this wave field's directional variation. The question now arises as to whether or not the deviation between the observed and predicted directions can be further reduced by implementing a wave/current interaction model.

For the case being studied, as the waves enter the Gulf Stream, they are first refracted in a clockwise direction as they encounter an increasing velocity region of the current profile on the outer (eastern) edge of the Gulf Stream boundary. Similarly, they are refracted counterclockwise as they encounter the decreasing velocity region of the current profile on the inner (western) edge of the Gulf Stream. Based upon this kinematic model, unless total internal trapping or reflection occurs, the direction of a wave departing the influence of the Gulf Stream should be the same as when the wave entered the Gulf Stream. However, the point of departure of that wave ray will be displaced laterally from the position from which the wave ray would have emerged if it had not encountered the Gulf Stream. This distance was calculated to be on the order of 0.2 km for the conditions encountered during this study.

The refracted wave angles can be calculated by using Phillips' model as presented in (9). After a wave is generated by the hurricane, it is assumed to propagate in the same direction as the projected wave ray toward the Gulf Stream. After this wave enters the outer boundary of the stream, it is refracted as stated in Phillips' model. The projected wave ray directions from Hurricane Ella were used as input conditions into the wave/current interaction model. The average wave number, as measured by the SEASAT SAR, was also used as an input. New projected wave rays, at 1° increments, were calculated, and the SAR-observed directions were compared to the projected rays.

The projected wave rays are summarized in Table 2. The calculated wave/current interaction angle is nearly zero for the more southern wave rays and becomes larger as the incident angle (measured from east and counterclockwise) increases. The refraction angle is then added to or subtracted from its projected wave ray. This modified projected wave ray, which includes the effect of the Gulf Stream, can now be compared to the nearest SEASAT-observed wave ray (Figure 6). The results of this comparison are also shown in Table 2. The mean angu-

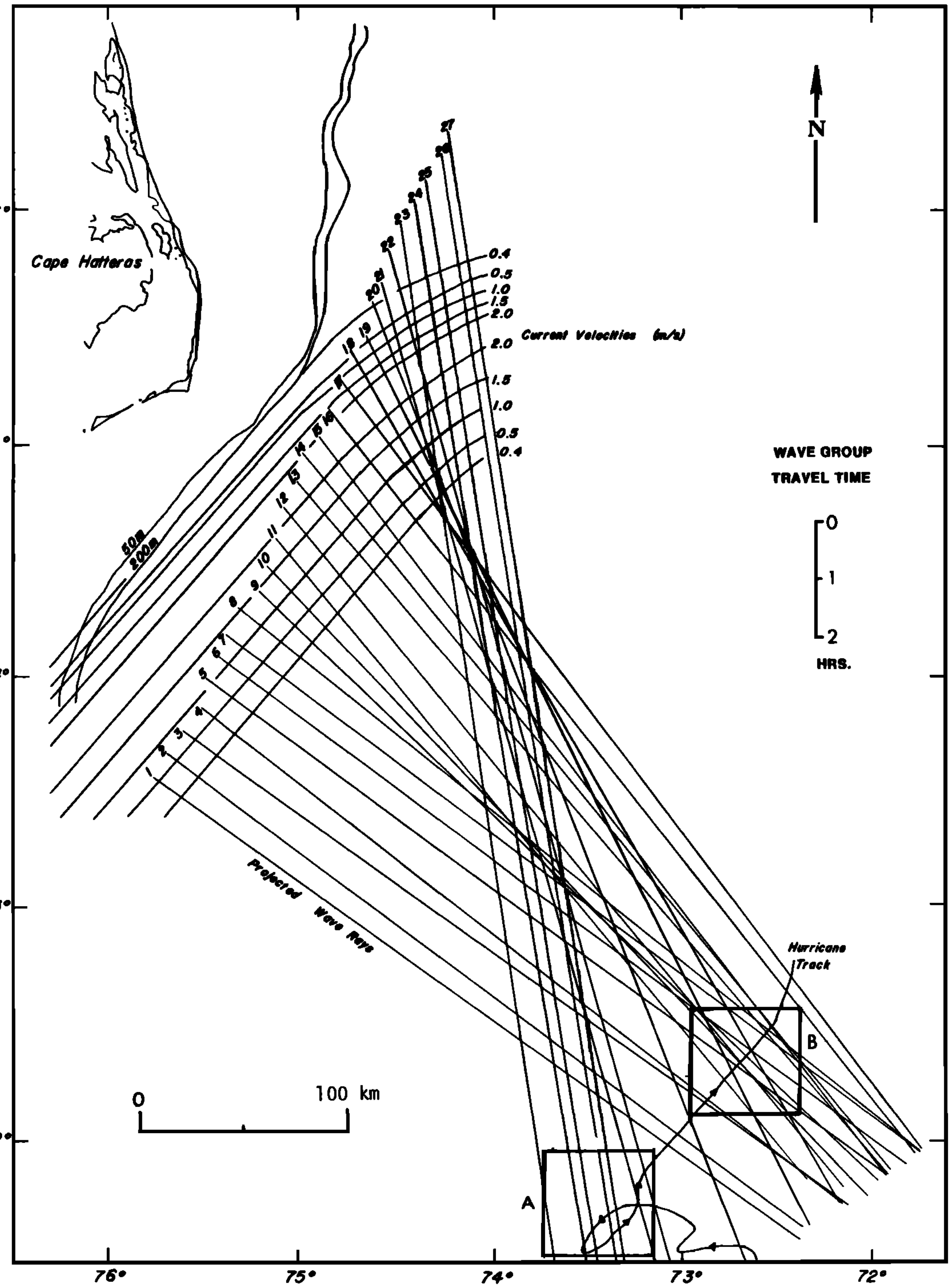


Fig. 5. Great circle wave ray hindcasts utilizing SEASAT SAR-derived wave characteristics to determine wave generation regions.

lar variation between the observed and calculated wave rays are on the order of 2.6° for group 1; 9.0° for group 2A; 6.2° for group 2B; and −5.9° for group 3.

Continuing the wave rays beyond the western boundary of the Gulf Stream places rays 12 to 17 into intermediate and eventually shallow water with respect to wavelength. To account for topographically induced wave refraction, these rays were numerically projected shoreward using a computer-based wave refraction model [*Poole et al.*, 1977). The observed wave ray directions presented in Table 2 and Figure 6 take into account this bottom-induced refraction.

It therefore appears that the model has not accounted for all inherent directional variation in the deepwater wave field. Several possible explanations exist for these observations. First, the purely kinematic wave/current interaction model utilized in this investigation most likely underestimates the amount of surface gravity wave modification by the Gulf Stream. Second, the actual position of the maximum velocity portion of the Gulf

TABLE 2. Comparison of SAR-Observed Wave Rays with Hurricane Ella Projected Wave Rays

| Wave Ray | Group | Direction* of Observed Wave Ray Corrected for Refraction of the Gulf Stream and Bottom Bathymetry, deg | | | | Direction* of Great Circle Projected Wave Ray, deg | | | | Angle Difference† Between Observed Wave Ray and Projected Wave Ray, deg | | | | Average Angle Difference, deg |
|---|---|---|---|---|---|---|---|---|---|---|---|---|---|---|
| | | *A* | *B* | *C* | *D* | *A* | *B* | *C* | *D* | *A* | *B* | *C* | *D* | |
| 1 | | 144.0 | 146.0 | 144.0 | 144.7 | 145.0 | 144.7 | 144.5 | 144.3 | −1.0 | 1.3 | −0.5 | 0.4 | 0.1 |
| 2 | | 144.0 | 139.5 | 145.2 | 145.5 | 142.3 | 142.3 | 142.3 | 142.3 | 1.7 | −2.8 | 3.2 | 2.9 | 1.3 |
| 3 | 1 | 146.0 | 146.0 | 144.5 | 145.5 | 140.1 | 140.3 | 140.4 | 140.5 | 5.9 | 5.7 | 4.1 | 5.0 | 5.2 |
| 4 | | 141.6 | 141.1 | 141.6 | 144.4 | 138.1 | 138.3 | 138.5 | 138.8 | 3.5 | 2.8 | 3.1 | 5.6 | 3.8 |
| | | | | | | | | | | | | | | 2.6‡ |
| 5 | | 142.6 | 142.1 | 142.9 | 144.9 | 135.8 | 136.1 | 136.5 | 136.7 | 6.8 | 10.0 | 6.4 | 8.2 | 7.9 |
| 6 | | 144.6 | 142.1 | 143.9 | 144.4 | 133.1 | 133.6 | 134.1 | 134.5 | 11.5 | 8.5 | 9.8 | 9.9 | 9.9 |
| 7 | 2A | 145.2 | 141.1 | 143.5 | 142.8 | 131.3 | 131.6 | 132.0 | 132.4 | 13.9 | 9.5 | 11.3 | 10.4 | 11.3 |
| 8 | | 143.7 | 141.4 | 140.3 | 140.3 | 130.1 | 130.3 | 130.5 | 130.6 | 13.6 | 11.1 | 10.0 | 9.7 | 11.1 |
| 9 | | 136.3 | 136.0 | 133.3 | 134.3 | 127.2 | 127.6 | 128.3 | 128.7 | 9.1 | 8.4 | 5.0 | 5.6 | 7.0 |
| 10 | | 134.0 | 132.0 | 131.5 | 133.5 | 126.0 | 126.1 | 126.4 | 126.5 | 8.0 | 5.9 | 5.1 | 7.0 | 6.5 |
| | | | | | | | | | | | | | | 9.0‡ |
| 11 | | 130.8 | 129.0 | 127.3 | 126.3 | 124.3 | 124.4 | 124.6 | 124.9 | 6.5 | 4.6 | 2.7 | 1.4 | 3.8 |
| 12 | | 129.4 | 126.9 | 124.4 | 128.6 | 121.9 | 122.0 | 122.4 | 122.6 | 7.5 | 4.9 | 2.0 | 6.0 | 5.1 |
| 13 | | 129.2 | 127.2 | 128.2 | 127.7 | 120.7 | 121.1 | 121.3 | 121.4 | 8.5 | 6.1 | 6.9 | 6.3 | 7.0 |
| 14 | | 125.7 | 126.7 | 124.0 | 127.8 | 118.9 | 119.0 | 119.4 | 119.7 | 6.8 | 7.7 | 4.6 | 8.1 | 6.8 |
| 15 | 2B | 121.7 | 125.9 | 124.5 | 127.4 | 118.0 | 118.1 | 118.4 | 118.6 | 3.7 | 7.8 | 6.1 | 8.8 | 6.6 |
| 16 | | 122.3 | 125.5 | 126.2 | 126.7 | 115.8 | 116.9 | 116.7 | 117.3 | 6.5 | 8.5 | 9.5 | 9.4 | 8.5 |
| 17 | | 124.0 | 127.2 | 125.9 | 126.2 | 114.9 | 115.0 | 115.2 | 115.4 | 9.1 | 12.2 | 10.7 | 10.8 | 10.7 |
| 18 | | 116.8 | 117.8 | 117.5 | 120.3 | 113.6 | 113.7 | 113.8 | 114.0 | 3.2 | 4.1 | 3.7 | 6.3 | 4.3 |
| 19 | | 114.9 | 114.9 | 113.9 | 117.9 | 111.8 | 112.0 | 112.2 | 112.4 | 3.1 | 3.9 | 1.7 | 5.5 | 3.3 |
| | | | | | | | | | | | | | | 6.2‡ |
| 20 | | 112.7 | 114.2 | 118.9 | 97.2 | 110.8 | 111.0 | 110.9 | 110.8 | 1.9 | 3.2 | 8.0 | −13.6 | −0.1 |
| 21 | | 110.3 | 105.3 | 102.8 | 102.0 | 110.2 | 110.1 | 109.9 | 109.4 | 0.1 | −4.8 | −7.1 | −7.4 | −4.8 |
| 22 | | — | 99.4 | 97.4 | 97.4 | — | 108.8 | 108.5 | 108.2 | — | −9.4 | −11.1 | −10.8 | −10.4 |
| 23 | | — | 102.5 | 97.5 | 96.5 | — | 108.0 | 107.4 | 107.2 | — | −5.5 | −9.9 | −10.7 | −8.7 |
| 24 | 3 | — | 101.6 | 97.6 | 97.1 | — | 106.7 | 106.2 | 106.1 | — | −5.1 | −8.6 | −9.0 | −7.6 |
| 25 | | 101.0 | — | 97.0 | — | 105.8 | — | 105.2 | 104.9 | −4.8 | — | −8.2 | — | −6.5 |
| 26 | | 101.0 | — | 97.0 | — | 104.8 | — | 104.2 | — | −3.8 | — | −7.2 | — | −5.5 |
| 27 | | — | — | — | — | — | — | — | — | — | — | — | — | — |
| 28 | | — | — | — | — | — | — | — | — | — | — | — | — | — |
| 29 | | — | — | — | — | — | — | — | — | — | — | — | — | — |
| | | | | | | | | | | | | | | 5.9‡ |

Dash indicates data not available.

*The direction is measured from the east and counterclockwise.

†Angle difference equals direction of observed wave ray corrected for refraction of the Gulf Stream and bottom bathymetry—direction of great circle projected wave ray.

‡The arithemetic average angle difference in each group.

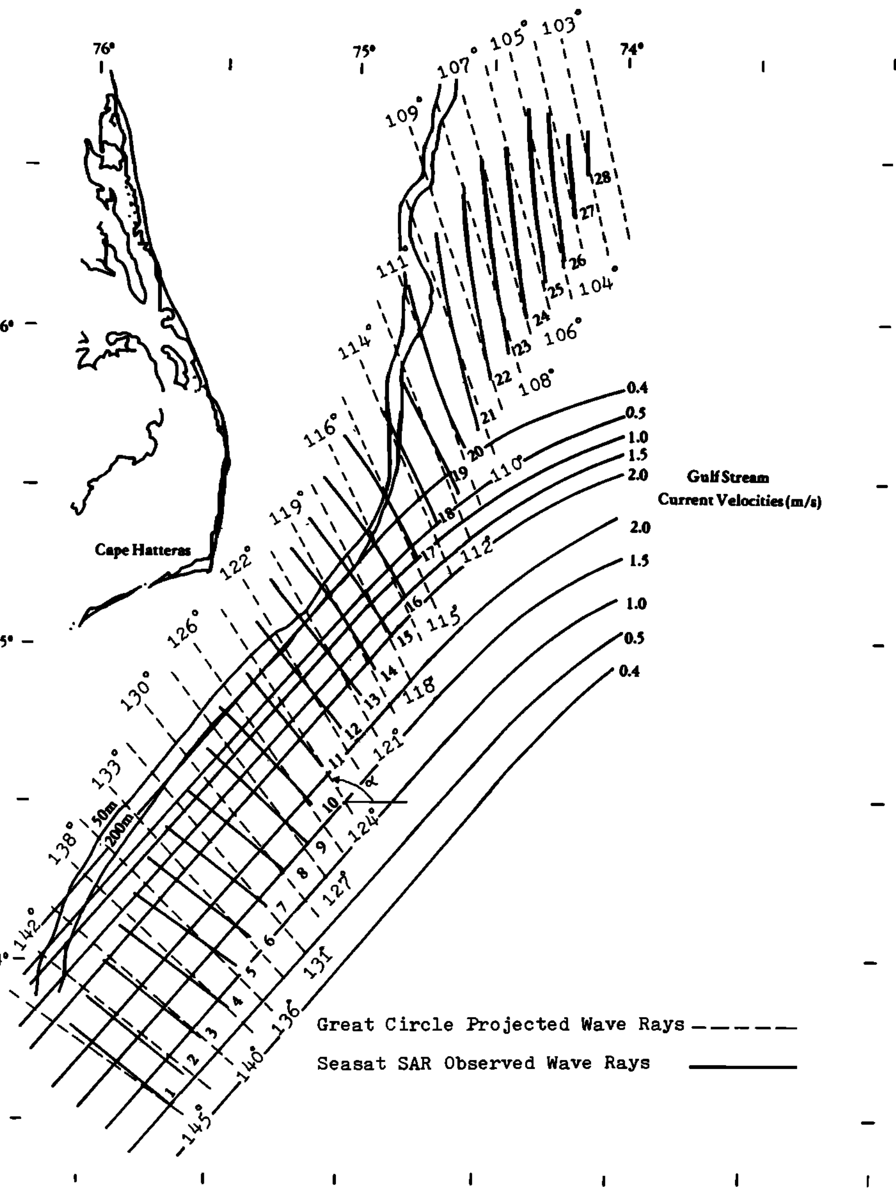


Fig. 6. Comparison between SAR-observed average wave rays and hurricane projected average wave rays including the calculated wave/current interaction provided by the Gulf Stream. The spatially averaged angle of the Great-Circle-projected wave rays is also indicated.

Stream may have been displaced more northerly than predicted by the U.S. Coast Guard for August 30, 1978. Third, it is likely there existed perturbations of the actual flow pattern of the Gulf Stream, such as rings and meanders, which were not resolved on the U.S. Coast Guard sea truth. Fourth, the input projected wave ray directions into the wave/current interaction model might actually vary spatially more than was first thought. Fifth, the vertical current shear of the Gulf Stream may have produced more severe wave refraction than predicted from this modeling effort. Any or all of these factors could have contributed the observed deviations between the SAR-sensed wave characteristics and those obtained from the wave/current interaction model.

## Calculation of Surface Currents by Observation of Wave Refraction

Perhaps the most useful application of this study of wave/current interaction is the quantification of the utility of SAR as a large-scale ocean surface current mapping tool. SAR-sensed subtle changes in the propagation characteristics—wave direction and dominant wave number—have the potential to be used to analytically solve for the gross velocity field of the upper region of the ocean. The assumptions employed in this formulation appear to be quite harsh, and they require further detailed investigation. However, in spite of this uncertainty the results obtained suggest that SEASAT SAR is capable of producing reliable estimates of large-scale ocean surface flow fields. The synoptic and repetitive coverage of large regions of the ocean surface that is provided by a satellite-borne radar system renders this technique extremely valuable as an eventual operational tool.

As previously presented, *Phillips* [1981] suggests that conservation of wave number for propagation through a nonstationary medium requires the use of (3) to calculate the apparent wave frequency. Alternately, (3) can be rewritten as

$$\sigma_0 = \sigma + ku \cos \alpha = \text{constant} \qquad (10)$$

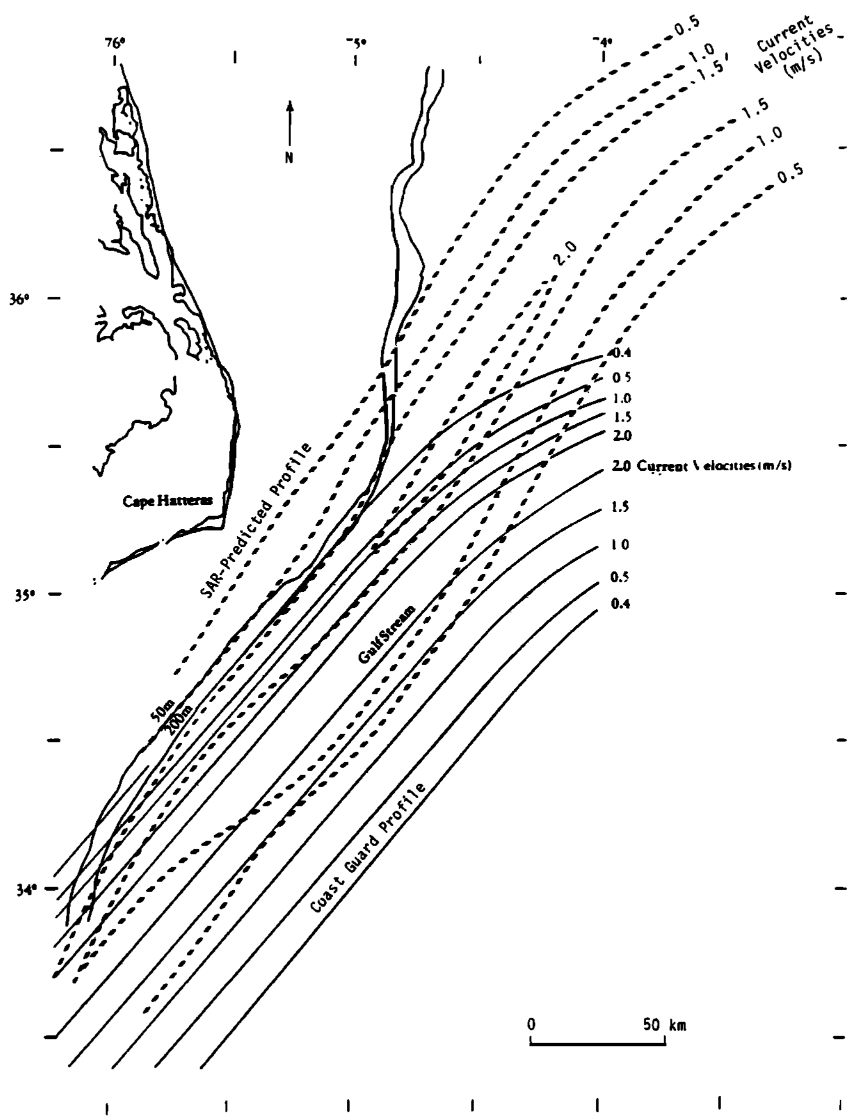


Fig. 7. Comparison of SAR-derived Gulf Stream surface current velocities with U.S. Coast Guard predicted current profile.

where $k$ is the local wave number ($k = 2\pi/L$), $u$ is the flow velocity of the upper region of the ocean, $\sigma_0$ is the apparent wave frequency measured at a fixed point in a fluid assumed to be at rest, $\sigma$ is the wave frequency ($\sigma = 2\pi/T$) observed in the moving fluid, and $\alpha$ is the angle between the local current and wave number vectors.

The two most directly observable characteristics of wave propagation from spaceborne SAR are the propagation direction and wave number of the dominant gravity wave components. As previously demonstrated, both of these quantities should be altered as a result of wave/current interactions, and hence they offer possible indicators of the underlying flow structure of the upper ocean. Published values for the absolute resolution of the dominant-wave-component direction from spaceborne SAR [*Vesecky and Stewart*, 1982] indicate reliable estimates can be obtained to within $\pm 11°$ absolute for wave direction of propagation and $\pm 15\%$ for dominant wavelength when compared with conventional ocean surface measurements. For the present analysis, however, it is only necessary to compare wavelengths and directions between points in the same SAR scene. Therefore, an error analysis was conducted during the present study to determine the relative accuracy of the OFT method. This analysis considered not only the precision of the OFT technique but also the sources of variation in the method. A statistical analysis of the relative accuracy and reliability of the OFT estimates indicated that the SAR is capable of producing an estimate of the relative wave propagation direction to within 1.2°. A similar estimate for SAR-sensed gravity wave numbers was obtained to a relative accuracy of approximately 2%. Relative accuracies refer to the SAR's ability to detect change from one 44 $km^2$ transform area to another. Further error analysis indicated that two OFT positions had to have an absolute difference of 5 m in wavelength and 1.0° in wave direction before they could be considered statistically different. The calculated changes in incident wave direction as a result of waves from Hurricane Ella crossing the Gulf Stream range from a few tenths of a degree to only a few degrees. Since the anticipated wave direction changes will be small, an analytical formulation that eliminates the angular change in wave propagation was chosen. This was accomplished by employing the following two stringent assumptions: First, the resulting change in wave direction from interaction with the Gulf Stream is assumed small (less than a few degrees); second, all straining in the wave $k$ vector field that results from the Gulf Stream is assumed to originate from only the current component in the direction of wave propagation, and the orthogonal components of this strain can be treated independently. Employing these assumptions, changes in the direction of propagation of the dominant wave components can be analytically eliminated from this formulation.

From conservation of wave number components, for a current varying in the cross-stream direction ($y$ direction):

$$k \cos \alpha = k_0 \cos \alpha_0 \qquad (11)$$

where again, the subscript 0 denotes the parameter value in the undisturbed fluid.

Combining (10) and (11), and assuming that the total amount of straining induced in the surface wave field is the result of only the current component in the direction of wave propagation ($\alpha_0 = \alpha = 0$), gives the following expression for $u$, the velocity of the underlying fluid required to produce the observed change in wave propagation characteristics:

$$u^2 = \frac{(\sigma_0 - \sigma)^2\left[1 - \left(\frac{k_0}{k}\right)^2\right]}{k^2 - k_0^2} \qquad (12)$$

or

$$u = \frac{(gk_0)^{1/2} - (gk)^{1/2}}{k} \qquad (13)$$

Utilizing this formulation and the wave number vectors of the dominant wave components resolved by the OFT analysis, orthogonal components of the current field of the Gulf Stream were calculated. These two orthogonal components are in the satellite cross-track and along-track direction. A total of 99 OFT's were used in this calculation. The resulting vector magnitudes of the calculated upper ocean flow field were then obtained. At each OFT location the total current magnitudes were then smoothed with a three-point moving average (corresponding to a spatial resolution of 34 km) in the along-track direction and contoured on 0.5 m/s intervals to produce a visualization of the upper-ocean flow structure. The agreement between these SAR-derived velocities and those published by the U.S. Coast Guard for the time of this SEASAT overpass (Figure 7) are in general agreement; however, the western boundary of the Gulf Stream is no longer situated at the 200-m depth contour.

## SHALLOW-WATER WAVE REFRACTION

An additional aspect of this analysis of a SAR-imaged, spatially envolving gravity wave field was to utilize the deepwater, Gulf-Stream-perturbed wave field as input into a shallow wave refraction study. A comparison between Airy shallow-water wave theory and the SAR-derived dominant wavelengths and directions will be presented. This favorable comparison serves as further confirmation that the SEASAT SAR successfully imaged subtle changes in this wave field and that the sensed changes in wave propagation characteristics agreed well with theory.

It is not the intent of this paper to present in detail the results of the shallow-water wave refraction study for the Cape Hatteras, revolution 974 data set. In a previous analysis of this data set it was assumed that a homogeneous deepwater gravity wavefield was present in this area [*Shuchman and Kasischke*, 1981]. It is now recognized, because of this detailed deep wave wave/current interaction analysis, that this assumption was not valid and that new, varying, deepwater wavelengths and directions were necessary as inputs for the shallow-water wave refraction models. Thus 11 subgroups were defined to minimize the variation in the deepwater wavelength and direction. These subgroups are illustrated in Figure 8. The deepwater positions chosen for each subgroup were defined so as to include those points closest to the 200-m contour but still in deep water (>200 m). The wavelength and direction data for these points were then averaged for each subgroup and are summarized in Table 3.

Using these new deepwater inputs, two wave refraction models were used to evaluate SEASAT's ability to monitor changes in the gravity wave field as it propagates into shallow water. The first model is the wavelength comparison model based on Airy wave theory. The second model was a computer-based model obtained from NASA and is described in detail by *Poole et al.* [1977]. The depth values used for inputs to both

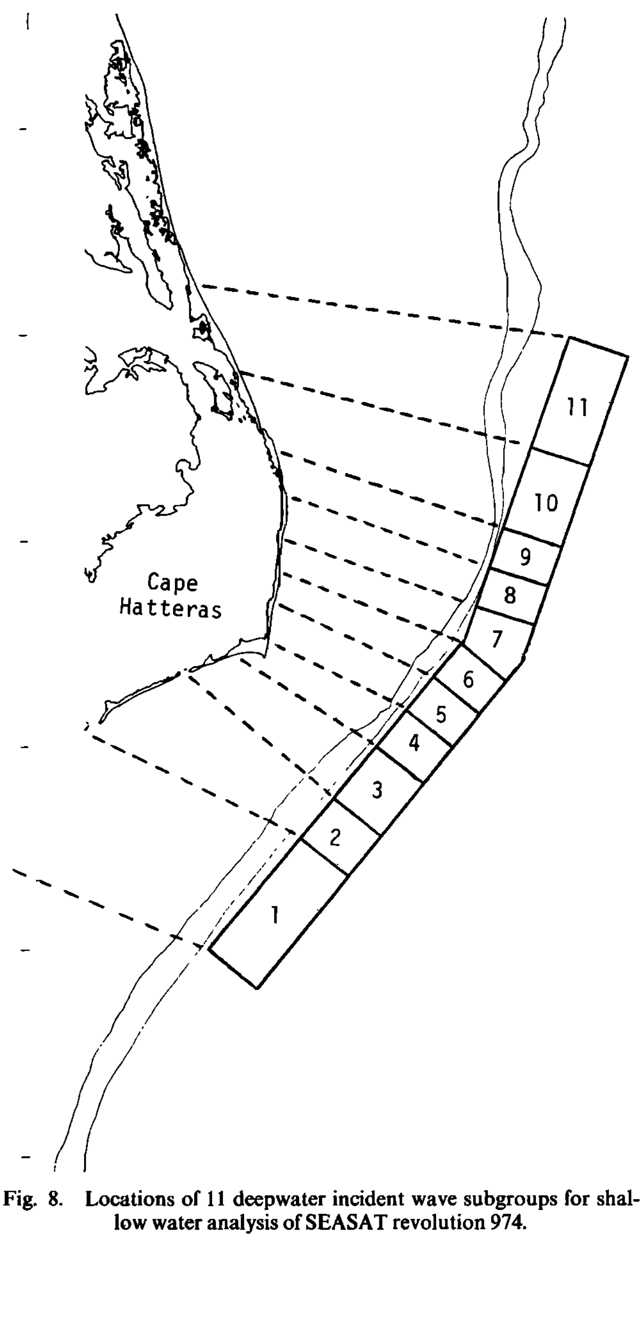


Fig. 8. Locations of 11 deepwater incident wave subgroups for shallow water analysis of SEASAT revolution 974.

TABLE 3. Dominant Wavelengths and Directions for Deepwater Subgroups

| Subgroup | Points | $\lambda$, m | $\theta$ |
|---|---|---|---|
| 1 | 9D, 10D, 11D | 196.4 | 313.2° |
| 2 | 11D, 12C | 192.2 | 318.3° |
| 3 | 12C, 13C | 189.8 | 322.3° |
| 4 | 13C, 14B | 193.3 | 321.5° |
| 5 | 14B, 15B | 195.7 | 320.5° |
| 6 | 15B, 16B | 195.7 | 321.8° |
| 7 | 16B, 17B | 198.8 | 321.8° |
| 8 | 17B, 18B | 195.1 | 325.5° |
| 9 | 18B, 19B | 188.7 | 330.3° |
| 10 | 19B, 20C | 183.2 | 330.5° |
| 11 | 20C, 21D | 185.3 | 330.5° |

models were obtained from the NOAA/EDIS digital bathymetry tapes.

Figure 9 summarizes the model-predicted wavelengths versus the SAR-observed wavelengths for the two models. It can be seen that the wave refraction model predicted longer wavelengths than were observed with the SEASAT SAR.

Similarly, Figure 10 summarizes the estimates of dominant wave direction of propagation as generated by the computer wave refraction model compared with the SAR-derived estimates. As with the previous study of this data [*Shuchman and Kasischke*, 1981], the directions produced by the SAR did not fit the wave refraction model results as well as the wavelength comparisons. A trend in the data is present but not strong.

One trend in the wave refraction analyses above was that the waves detected by the SAR had shorter wavelengths than were predicted by the wave refraction model. One of four reasons could account for this: (1) A bias exists in the manner the SAR observes gravity waves. (2) The water depths were less than the chart values. (3) A physical disturbance was present which decreased the wavelength a greater amount than would occur naturally. (4) A bias exists in the manner in which the SAR images shoaling gravity waves. Previous studies of the ability of the SEASAT SAR to estimate dominant wavelength have not detected a bias in the SAR data [*Shuchman et al.*, 1981]. The depth data to which comparisons were made were from actual hydrographic surveys and are not suspect, but they are known to be conservative. Some oceanic factor could be the cause. In the region of the eastern U.S. coastline, a countercurrent (to the Gulf Stream) is well documented. This current generally flows in a southerly direction and could be responsible for shortening the wavelengths in the nearshore coastal region of Cape Hatteras. Finally, a bias in the way the SAR is imaging the waves in coastal waters could exist because of the nonstationary nature of gravity waves in shallow water.

The results obtained from the wavelength comparison between SAR-observed values and the two model estimates were

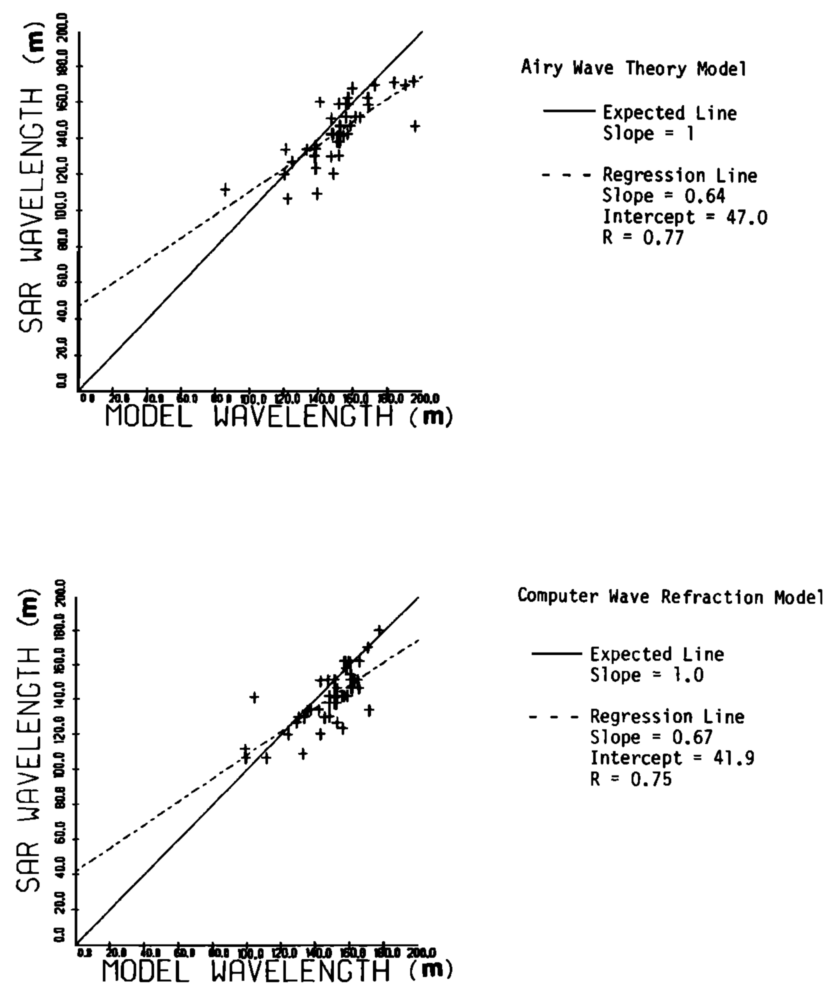


Fig. 9. Comparison of dominant wavelengths from the Airy wave theory and computer wave refraction models with SAR-observed values.

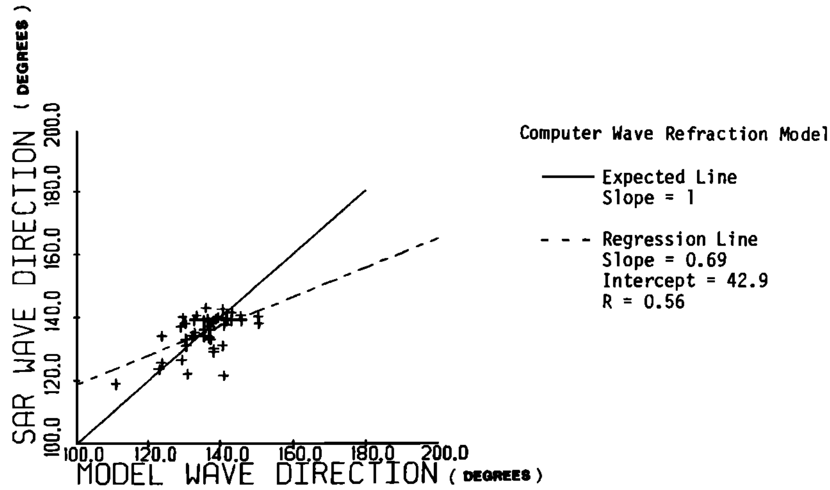


Fig. 10. Comparison of dominant wave propagating directions from computer wave refraction model with SAR-observed values.

essentially the same (see Figure 9). The best linear fits to the data all have a slope of approximately 0.65 and a $y$ intercept of 45 m. If the SAR were truly imaging the gravity waves, we would expect better agreement than this. Previous analyses of the ability of the SEASAT SAR suggest that when the dominant ocean wavelength is on the order of 120 m or less, the SAR has difficulty imaging these waves [*Kasischke*, 1980]. We therefore have some justification for removing data points where the wave refraction models predict a wavelength of 120 m or less. This was done for the Cape Hatteras data set, and new wavelength comparisons made. These results indicate that the slope of the regression equation is now between 0.82 and 0.91, with a $y$ intercept between 5 and 19 m, as seen in Figure 11.

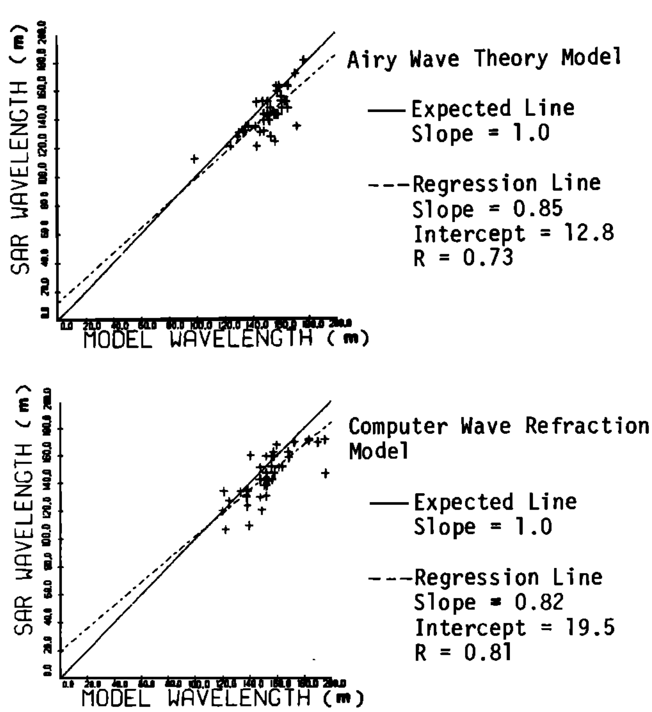


Fig. 11. Airy wave theory and computer wave refraction model predicted wavelengths versus SAR-observed wavelengths, eliminating values where the SAR detected wavelength was less than 120 m.

## SUMMARY

This investigation represents a further attempt to document and predict subtle changes in the propagation characteristics of a hurricane-generated evolving gravity wave system. As a result of these efforts, several significant surface gravity wave and oceanographic phenomena have been investigated over a large spatial region of the ocean. The primary significance of this study is the documentation of the variation in gravity wave fields over a large area. This documentation was realized by generating a large number of two-dimensional optical Fourier transforms of the SAR-observed sea surface as well as collecting ancillary environmental data of the test site. By employing spectral analysis techniques which provide high-resolution data with respect to dominant wave number and direction, it was possible to ascertain the following information on the wave field imaged during SEASAT revolution 974: (1) the wave-generation region of Hurricane Ella by wave ray hindcasting to a 50-km$^2$ region; (2) nonuniform deepwater wave conditions away from the wave generation region; (3) subtle changes in gravity wavelength and direction as a result of wave/current interactions with the Gulf Stream; and (4) SEASAT-SAR-derived changes in wave propagation characteristics to analytically solve for the gross flow field of the upper ocean.

This investigation has demonstrated that through the use of a large number of OFT's, very reliable estimates of wave propagation characteristics and their spatial gradients can be obtained. These same procedures should also be attempted for digital Fourier transforms of SEASAT SAR digitally processed data. This study has also demonstrated the potential of detecting the dynamics of the upper ocean, utilizing SAR-sensed changes in the gravity wave field structure. Should this technique prove reliable with other SEASAT SAR data sets, a potential for rapid, global surface current mapping may exist. Refinement of the techniques and analytical formulations employed in this investigation may eventually lead to an operational, global ocean sensing capability for storm-wave-generation regions, and/or ocean surface currents and near-shore bathymetric changes.

*Acknowledgments.* This study was jointly supported by the National Oceanic and Atmospheric Administration (NOAA) and the National Aeronautics and Space Administration (NASA) as part of the SEASAT Announcement of Opportunity Program under contract

MO-A01-78-00-4339. The technical monitors for this contract were John W. Sherman III and Patrick Deleonibus of NOAA.

This study would not have been possible without the cooperation and efforts of many people. It is a pleasure to acknowledge the help of the following individuals: R. Shounia of ERIM generated all the optical Fourier transforms; Vincent J. Cardone of Ocean Weather, Inc., and Duncan Ross of NOAA's Sea-Air Interaction Laboratory provided their expertise on Hurricane Ella; Benjamin Holt of the Jet Propulsion Laboratory provided SEASAT SAR data from revolution 974; James Hammack of the Defense Mapping Agency, Hydrographic Center, provided information and bathymetric charts for the test sites; personnel of the Physical Oceanography Laboratory of the Department of Atmospheric and Oceanic Science, University of Michigan, provided technical comments and support for this study; and D. Lyzenga and J. Lyden of ERIM reviewed the technical contents of this study.

## REFERENCES

Beal, R. C., P. S. Deleonibus, and I. Katz (Eds.), *Spaceborne Synthetic Aperture Radar for Oceanography*, 215 pp., Johns Hopkins Press, Baltimore, 1981.

Brown, W. M., and L. Porcello, An introduction to synthetic aperture radar, *IEEE Spectrum*, *6*, 52–66, 1969.

Fuglister, F. C., Gulf Stream '60, in *Progress in Oceanography*, vol. 1, edited by M. Sears, pp. 265–373, Macmillan, New York, 1963.

Fuglister, F. C., and L. V. Worthington, Some results of a multiple ship survey of the Gulf Stream, *Tellus*, *3*, 1–14, 1951.

Gonzalez, F. I., R. C. Beal, W. E. Brown, P. S. Deleonibus, J. W. Sherman, J. F. R. Gower, D. Lichy, D. B. Ross, C. L. Rufenach, and R. A. Shuchman, Seasat synthetic aperture radar: Ocean wave detection capabilities, *Science*, *204*, 1418–1421, 1979.

Harger, R. O., *Synthetic Aperture Radar Systems*, 240 pp., Academic, New York, 1970.

Hayes, J. G., Ocean current wave interaction study, *J. Geophys. Res.*, *85*, 5025–5031, 1981.

Iselin, C. O. D., A study of the circulation of the western North Atlantic, *Pap. Phys. Oceanogr. Meteorol.*, *4*(4), 101, 1936.

Iselin, C. O. D., and F. C. Fuglister, Some recent developments in the study of the Gulf Stream, *JJ. Mar. Res.*, *7*, 317–329, 1948.

Jordan, R. L., The Seasat-A synthetic aperture radar system, *IEEE J. Oceanic Eng.*, *OE-5*, 154–164, 1980.

Kasischke, E. S., Extraction of gravity wave information from synthetic aperture radar data, M.S. thesis, 108 pp., Univ. Mich., Ann Arbor, 1980.

Kasischke, E. S., R. A. Shuchman, G. A. Meadows, P. L. Jackson, Y. Tseng, J. D. Lyden, Further Seasat Coastal Ocean Wave Analysis, *Final Rep. 138600-6-F*, 189 pp., Environ. Res. Inst. Mich., Ann Arbor, 1981.

Kenyon, K. E., Wave refraction in ocean currents, *Deep-Sea Res.*, *18*, 1023–1034, 1971.

Lake, B. M., and H. C. Yuen, A new model for nonlinear gravity waves, 1, *J. Fluid Mech.*, *88*, 33–62, 1978.

Longuet-Higgins, M. S., The instabilities of gravity waves of finite amplitude in deep water, 1, Superharmonics, *Proc. R. Soc. A*, 471–488, 1978.

Longuet-Higgins, M. S., and R. W. Stewart, Changes in the form of short gravity waves on long waves and tidal currents, *J. Fluid Mech.*, *8*, 565–583, 1960.

Meadows, G. A., R. A. Shuchman, and J. D. Lyden, Analysis of remotely sensed long-period wave motions, *J. Geophys. Res.*, *87*, 5731–5740, 1982.

Peregrine, D. H., Interaction of water waves and currents, *Advan. Appl. Mech.*, *16*, 9–117, 1976.

Phillips, O. M., The structure of short gravity waves on the ocean surface, in *Spaceborne Synthetic Aperture Radar for Oceanography*, edited by R. C. Beal, P. S. DeLeonibus, and I. Katz, pp. 24–31, Johns Hopkins Press, Baltimore, 1981.

Poole, L. H., S. R. LeCroy, and W. D. Morris, Minimal-resource computer program for automatic generation of ocean wave ray or crest diagrams in shoaling water, *Tech. Memo. 74076*, NASA Langley Research Center, Hampton, Va., 1977.

Richardson, P. L., and J. A. Knauss, Gulf Stream and western boundary undercurrent observations at Cape Hatteras, *Deep-Sea Res.*, *18*, 1971.

Schwab, D. J., R. A. Shuchman, and P. L. Liu, Wind wave directions determined from synthetic aperture radar imagery and from a tower in Lake Michigan, *J. Geophys. Res.*, *86*, 2059–2064, 1981.

Shuchman, R. A., Quantification of SAR signatures of shallow water ocean topography, Ph.D. dissertation, 130 pp., Univ. Mich., Ann Arbor, 1982.

Shuchman, R. A., and E. S. Kasischke, Refraction of coastal ocean waves, in *Spaceborne Synthetic Aperture Radar for Oceanography*, edited by R. C. Beal, P. S. Deleonibus, and I. Katz, pp. 128–135, Johns Hopkins Press, Baltimore, 1981.

Shuchman, R. A., and G. A. Meadows, Airborne synthetic aperture radar observations of surf zone conditions, *Geophys. Res. Lett.*, *7*, 857–860, 1980.

Shuchman, R. A., E. S. Kasischke, A. Klooster, and P. L. Jackson, SAR coastal ocean wave analysis—A wave refraction and diffraction study, *Final Rep. 138600-2-F*, 78 pp., Environ. Res. Inst. Mich., Ann Arbor, 1979.

Shuchman, R. A., E. S. Kasischke, J. D. Lyden, and G. A. Meadows, The use of synthetic aperture radar (SAR) to measure ocean gravity waves, in *Proceedings of the National Academy of Sciences Special Conference on Wave-Measurement Technology*, pp. 95-111, National Academy Press, Washington, D. C., 1982.

Vesecky, J. F., and R. H. Stewart, The observation of ocean surface phenomena using imagery from the Seasat synthetic aperture radar—An assessment, *J. Geophys. Res.*, *87*, 3397–3430, 1982.

U.S. Coast Guard, Weekly Sea Current Chart Production Manual, *Tech. Rep. 78-3*, Oceanogr. Unit, U.S. Coast Guard, Dep. Transport. Washington, D. C., 1978.

Von Arx, W. S., *An Introduction to Physical Oceanography*, 422 pp., Publishing Company, Inc., Reading, Mass., 1962.

Worthington, L. V., Three detailed cross sections of the Gulf Stream, *Tellus*, *6*, 116–123, 1954.

Yuen, H. C., and B. M. Lake, Instabilities of waves on deep water, *Ann. Rev. Fluid Mech.*, *13*, 303–334, 1980.

(Received July 21, 1982;
revised December 7, 1982;
accepted December 7, 1982.)